Hindawi Publishing Corporation
International Journal of Photochemistry
Volume 2015, Article ID 790153, 9 pages
http://dx.doi.org/10.1155/2015/790153

Research Article

Synthesis, Characterization, and Visible Light Photocatalytic Activity of Nanosized Carbon Doped Zinc Oxide

A. B. Lavand and Y. S. Malghe

Department of Chemistry, The Institute of Science, 15 Madam Cama Road, Mumbai 400032, India

Correspondence should be addressed to Y. S. Malghe; ymalghe@yahoo.com

Received 10 September 2014; Revised 24 December 2014; Accepted 25 December 2014

Academic Editor: Shinya Maenosono

ZnO precursor was prepared using microemulsion method. Precursor was calcined in a furnace in a temperature range of 300–500°C with an interval of 100°C. Precursor and calcined nanopowders were characterized using TG/DTA, XRD, FT-IR, EDX, TEM, SEM, and particle size analyzer. Precursor calcined at 300°C for 2 h contains 3.87% carbon (C). Increase in calcination temperature of precursor shows decrease in C content. Precursor calcined at 500°C for 2 h yielded pure ZnO. UV-visible spectrophotometer was used to analyze the concentration of MG during the degradation process. In presence of visible light C doped ZnO obtained by calcining precursor at 300°C shows better photocatalytic activity for MG degradation. Parameters affecting the photocatalytic process such as calcination temperature of catalyst, catalyst loading, MG concentration, and pH of solution have been investigated.

1. Introduction

Environmental pollution has become a major threat to the human lives. Pollutants from polluted air and industry effluents create severe ecological problems. Photocatalytic oxidation of organic pollutants from industrial waste water by using semiconducting oxides can be an alternative to conventional methods for environmental remediation. Due to its mild operating conditions and the fact that it can be powered by sunlight, it allows green mineralization of organic pollutants [1–4]. Among the semiconductors TiO_2 photocatalyst has been extensively investigated. Anatase TiO_2 shows better photocatalytic activity and is used as photocatalyst. It is difficult to prepare phase pure anatase TiO_2, and also preparation of TiO_2 is costly. Zinc oxide (ZnO) can be considered as a suitable alternative to TiO_2 photocatalyst due to its nontoxic nature, good environmental stability, strong oxidizing power, and same band gap energy and is relatively cheaper. The major advantage of ZnO is that it absorbs a large fraction of solar spectrum than TiO_2 [5–7]. ZnO has been used for the photodegradation of various dye pollutants [8–10]. ZnO has a wide band gap of about 3.2 eV and can absorb UV light with wavelength below 387 nm, due to the fact that its photocatalytic activity is limited to irradiation wavelength in UV region only. Unfortunately, solar light consists of less than 5% UV radiations and indoor lighting consists of less than 0.1% UV radiations. Therefore it is necessary to modify ZnO in order to utilize major portion of sunlight/indoor lights.

For the development of visible light sensitive ZnO several methods are used. It includes dye sensitization [11, 12], semiconductor coupling [13, 14], metal or nonmetal doping [15–19], surface organic coating [20], and surface hybridization of ZnO with carbon [21]. Doping of ZnO with nonmetals such as carbon (C), nitrogen (N), and sulfur (S) leads to the formation of intermediate energy level between the band gap, enabling it to absorb visible light [22, 23]. Among the nonmetal dopants, C has been found to be very efficient for visible light induced photocatalysis. Its additional advantage is that it can promote the separation of photoelectrons and holes by channelizing the photoexcited electrons to nanosized C on the surface of catalyst, thereby reducing the rate of recombination [24–26].

In this paper we report the synthesis of C doped ZnO nanorods by reverse microemulsion method. Also its photocatalytic activity is examined for the degradation of MG in presence of visible light as a model photocatalytic reaction.

2. Experimental

2.1. Materials. Malachite green (MG) (bis[p-dimethylaminophenyl]phenyl-methylium oxalate) was obtained from Merck Chemicals, Mumbai, and used without any further purification. Zinc nitrate hexahydrate ($Zn(NO)_3{\cdot}6H_2O$), cyclohexane, n-butanol, N,N,N-cetyl trimethyl ammonium bromide (CTAB), acetone, ferric nitrate nanohydrate ($Fe(NO_3)_3{\cdot}9H_2O$), sodium hydroxide (NaOH), and ethanol used for the synthesis are of AR grade. All these chemicals were procured from SD Fine Chemicals, Mumbai, and used without further purification.

2.2. Synthesis of Precursor. 1 M solution of zinc nitrate was prepared by dissolving 29.74 g of $Zn(NO_3)_2{\cdot}6H_2O$ in 100 mL distilled water. 2 M sodium hydroxide solution was prepared by dissolving 8 g of NaOH in 100 mL distilled water. To 28.8 mL 1 M zinc nitrate, 35.5 mL cyclohexane, 8 mL butanol, and 5.90 g cetyltrimethylammonium bromide (CTAB) were added. In another solution 28.8 mL 2 M NaOH, 35.5 mL cyclohexane, 8 mL butanol, and 5.90 g CTAB were mixed. Both these solutions were stirred continuously with the help of magnetic stirrer to form clear solutions. These clear solutions were mixed with each other. The mixture was transferred to 250 mL Teflon lined autoclave and heated in an oven at 150°C for 1 h. After 1 h autoclave was cooled to room temperature. The solid product formed was separated by filtration, washed with distilled water followed by ethanol and finally with acetone, and dried in an oven at 60°C. The hydrothermal product (precursor) thus obtained was characterized using various characterization techniques.

2.3. Characterization. TG and DTA curves of precursor were recorded using simultaneous TG/DTA recording system (Rigaku, Model-Thermo Plus TG8120). For recording TG/DTA curves 14.20 mg precursor was heated in a nitrogen atmosphere with a heating rate 10°C min^{-1}. For recording DTA curve, alumina was used as a reference material. FT-IR spectra of precursor and the precursor calcined at 300, 400, and 500°C were recorded using FT-IR spectrophotometer (Bruker). Precursor was calcined at 300, 400, and 500°C for 2 h and the XRD patterns of the product obtained at different temperatures were recorded using X-ray diffractometer (Rigaku, Model-Miniflex II) using monochromatized CuKα radiation ($\lambda = 0.15405$ nm) with scanning rate of $2^\circ 2\theta$ min^{-1}. Qualitative elemental analysis was carried out using energy dispersive X-ray spectroscopy (EDX) (JEOL-JSM6360A) technique. TEM images of C doped/pure ZnO powder prepared in the present work were recorded using transmission electron microscope (Philips, CM200). For TEM sample was prepared by dispersing C doped/pure ZnO powder in isopropyl alcohol and solution was sonicated for 15 min. The drop of solution was placed over C coated copper grid and solvent was evaporated off under IR lamp. Particle size distribution study of product obtained at 300°C was carried out using particle size analyzer (Nanosight, Model-NTA-LM-20). Band gap energies of synthesized nanopowders were evaluated from UV-visible spectra recorded using UV-visible spectrophotometer (Shimadzu, Model-1800).

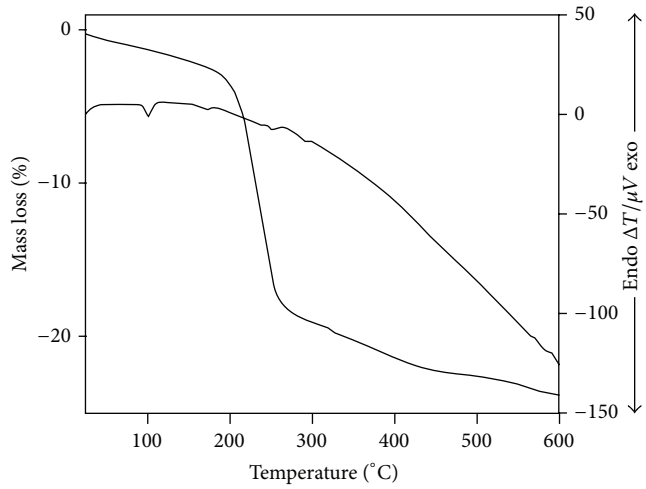

Figure 1: TG and DTA curves of ZnO precursor recorded in flowing nitrogen.

2.4. Photocatalytic Activity Study. Photocatalytic activity of nanosized pure/C doped ZnO photocatalyst was tested for degradation of malachite green (MG) solution. Reaction suspension was prepared by adding 0.05 g ZnO (obtained at 300°C) photocatalyst in 100 mL, 10 ppm MG solution. This aqueous suspension was stirred in the dark for 30 min to attain adsorption-desorption equilibrium. Later, the solution was irradiated with visible light. The visible light irradiation was carried out in a photoreactor using a compact fluorescent lamp (65 W, $\lambda > 420$ nm, Philips). Temperature of test solution was maintained constant throughout the experiment by circulating water around the solution. The amount of MG was monitored by sampling out 5 mL of aliquot solution at regular time intervals. The catalyst was first separated by centrifugation and the concentration of MG in the supernatant solution was estimated using UV-visible spectrum recorded in the wavelength range of 200–800 nm.

To evaluate the effect of various parameters on photocatalytic activity of ZnO, the same experiment was repeated by using the catalyst calcined at different temperatures, varying the amount of catalyst used, and changing the pH and concentration of MG.

3. Results and Discussion

3.1. TG and DTA Study. Simultaneous TG and DTA curves were recorded for thermal decomposition studies of precursor and are presented in Figure 1. TG curve shows that there is gradual weight loss from 25 to 200°C, and this can be attributed to vaporization of absorbed water molecules and cyclohexane. Also, this change is observed in DTA curve as an endothermic peak in the same temperature range with minima located near 104°C. In temperature range 200–330°C, TG curve exhibits a sudden weight loss, which corresponds to burning of residual surfactant and gives weak endothermic peak in DTA curve near 300°C.

Table 1: Properties of C doped and pure ZnO photocatalyst.

Sample	Calcination temperature (°C)	C content (%)	Band gap energy (eV)	Photodegradation efficiency (%) (irradiation time 60 min)
1	300	3.87	2.69	98
2	400	0.72	2.88	84
3	500	0	3.08	67

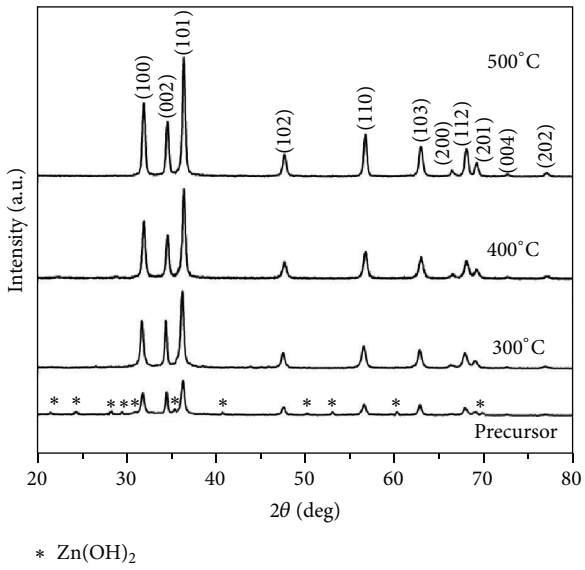

Figure 2: XRD patterns of precursor and precursor calcined at different temperatures.

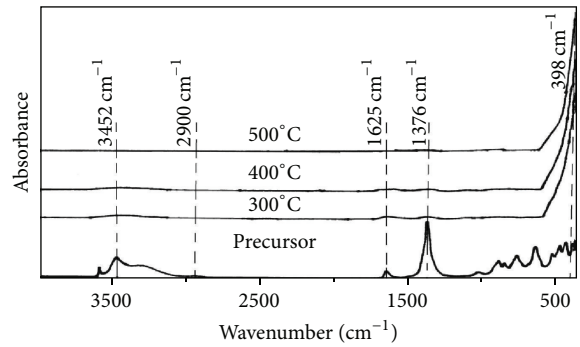

Figure 3: FT-IR spectra of precursor and precursor calcined at different temperatures.

Above 400°C there is no weight loss and TG curve gives a stable line. It indicates that precursor yields stable product above 400°C. This information was used to select the calcination temperature to get ZnO powder from its precursor. Precursor was calcined at 300, 400, and 500°C for 2 h and the product obtained was analyzed using X-ray diffractometer.

3.2. X-Ray Diffraction (XRD) Study. Figure 2 shows XRD patterns of precursor and product obtained after heating the precursor at 300, 400, and 500°C. XRD pattern of precursor shows that it is the mixture of $Zn(OH)_2$ and as-grown ZnO particles. These patterns suggest that product obtained by heating the precursor at different temperatures is crystalline in nature and is in good agreement with the wurtzite ZnO phase (JCPDS 36–1451). The average crystallite sizes of the product obtained were calculated from their XRD patterns using Debye-Scherrer equation and were found to be between 20 and 35 nm.

3.3. FT-IR Study. FT-IR spectra of the precursor and product obtained after calcinations of the precursor at different temperatures for 2 h are presented in Figure 3. It shows that precursor gives absorption peaks at 3452 and 1625 cm^{-1} which corresponds to the O–H stretching and bending vibration of the –OH bond [27]. It indicates that the precursor/hydrothermal product is the mixture of $Zn(OH)_2$ and as-grown ZnO particles. Peak at 1376 cm^{-1} can be assigned to C–O stretching in carbonyl. This information indicates that –OH and –C=O functional groups are present in precursor. This spectrum also shows absorption peaks below 560 cm^{-1} which corresponds to the stretching frequency of Zn–O bond in zinc oxide. FT-IR spectra of product obtained after heating the precursor at 300, 400, and 500°C for 2 h show no absorption peak in higher frequency region but give the sharp peak below 600 cm^{-1} which may be due to stretching frequency of Zn–O bond in zinc oxide. It indicates that precursor heated above 300°C for 2 h gives ZnO as a product.

3.4. Energy Dispersive X-Ray Spectroscopy (EDX) Study. EDX spectra of the precursor heated at various temperatures were recorded. From EDX spectra amount of C present in the sample was estimated and data obtained is presented in Table 1. It shows that C is present in the product obtained after calcining the precursor at 300 and 400°C and the amount of C is 3.87 and 0.72%, respectively (by weight). However the precursor heated at 500°C for 2 h yielded pure ZnO.

3.5. Transmission Electron Microscopy (TEM) Study. TEM images of precursor calcined at different temperatures were recorded and are presented in Figure 4. It shows that C doped ZnO prepared at 300°C is having a rod-like structure with diameter and length varying between 20–40 and 100–400 nm, respectively. Product obtained at 400°C is heterogeneous and consists of a mixture of rods and spheres. However ZnO particles obtained at 500°C are spherical in shape and size of particles ranges from 15 to 35 nm.

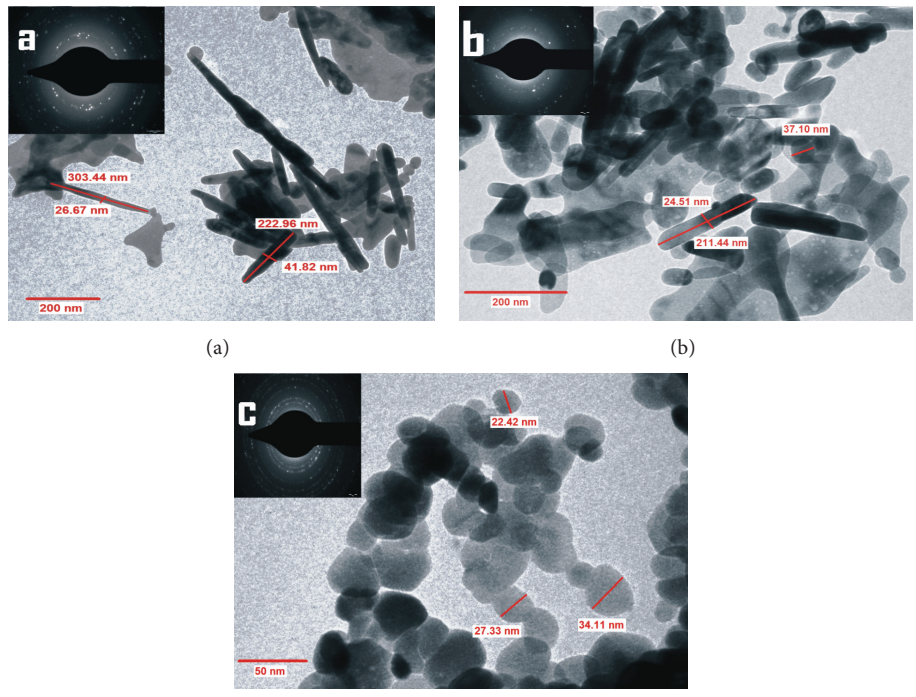

(a) (b)

(c)

Figure 4: TEM images of ZnO obtained at (a) 300, (b) 400, and (c) 500°C.

This is may be due to the addition of NaOH into aqueous solution of $Zn(NO_3)_2$ leads to the formation of white precipitate of $Zn(OH)_2$, which during hydrothermal treatment decomposes to ZnO. Thus the hydrothermal product obtained is a mixture of $Zn(OH)_2$ and as-grown ZnO particles. This mixture was heated in air and gives ZnO nanoparticles with different morphologies [26]. The probable reaction that occurred during thermal treatment could be given as

$$Zn^{2+} + 2OH^{-} \longrightarrow Zn(OH)_2\,(s) \xrightarrow{\text{Heating}} ZnO\,(s) + H_2O \quad (1)$$

Selected area electron diffraction patterns (SAED) of all the samples (inset) show distinct rings that correspond to the diffraction pattern of ZnO indicating crystalline nature.

3.6. Scanning Electron Microscopy (SEM) Study. SEM images of precursor calcined at different temperatures were recorded and are presented in Figure 5. It shows that C doped ZnO prepared at 300°C is having irregular shape. At 400°C this irregular shape initiated to transform into spherical shape and therefore it shows mixture of rods and spheres. ZnO particles obtained at 500°C are spherical in shape and at this temperature it shows aggregation.

3.7. Particle Size Analysis. Particle size distribution of ZnO synthesized in present work was studied using particle size analyzer. The particle size distribution curve for the precursor calcined at 300°C for 2 h is presented in Figure 6. This figure shows that particle size of C doped ZnO prepared in the present work varies over range from 20 to 70 nm with average particle size 43 nm, which is in agreement with the size obtained from TEM studies.

3.8. UV-Visible Spectrophotometery Study. UV-visible spectra of ZnO nanopowders synthesized in present work are presented in Figure 7. Figure 7(c) shows that pure ZnO (obtained at 500°C) gave band gap absorption edge at 403 nm whereas C doped ZnO, that is, ZnO obtained by calcining precursor at 400 and 300°C for 2 h, gave absorption peaks at higher wavelength whose absorption edges are at 430 and 461 nm, respectively. This distinct difference in absorption characteristics indicates that C is successfully doped on ZnO. The band gap energy of ZnO obtained at various temperatures was estimated using Tauc plot (Figure 8) and is presented in Table 1. The band gap energy of ZnO obtained at 300, 400, and 500°C is 2.69, 2.88, and 3.08 eV, respectively. Band gap of ZnO obtained at 300°C is less as compared to ZnO obtained at 400 and 500°C; due to this reason it absorbs higher wavelength (visible) light.

3.9. Visible Light Photocatalytic Activity Study. Visible light photocatalytic degradation of MG dye was studied in presence of nanosized pure and C doped ZnO. UV-visible spectra of aqueous solution of MG irradiated with visible light at different time intervals in presence of C doped ZnO (obtained at 300°C) were recorded and are presented in Figure 9. These spectra show characteristic peak maxima at 616 nm. As irradiation time increases the height of peak maxima at 616 nm decreases indicating photocatalytic degradation of

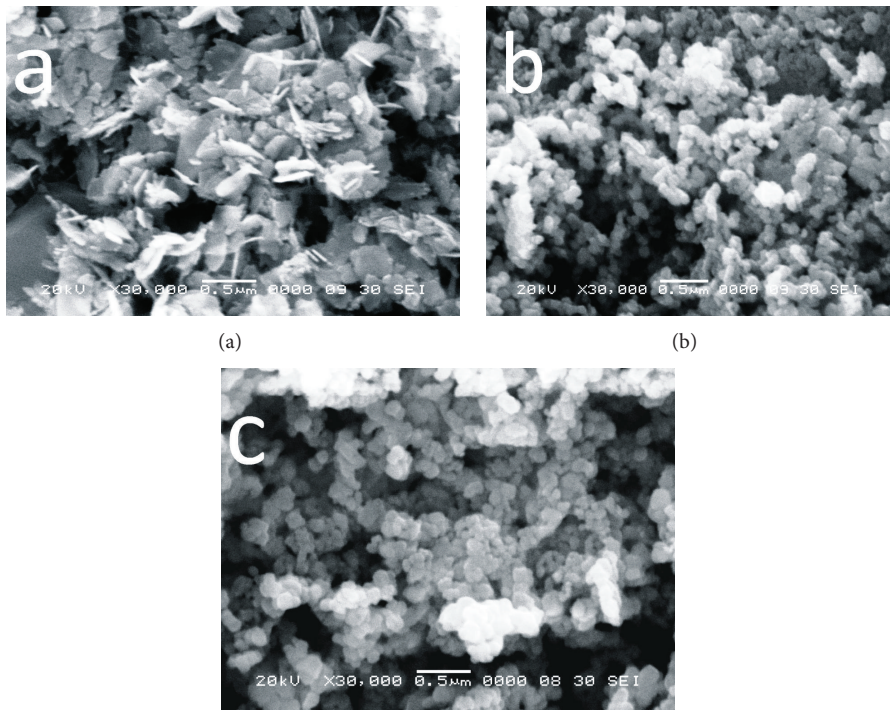

(a) (b)

(c)

Figure 5: SEM images of ZnO obtained at (a) 300, (b) 400, and (c) 500°C.

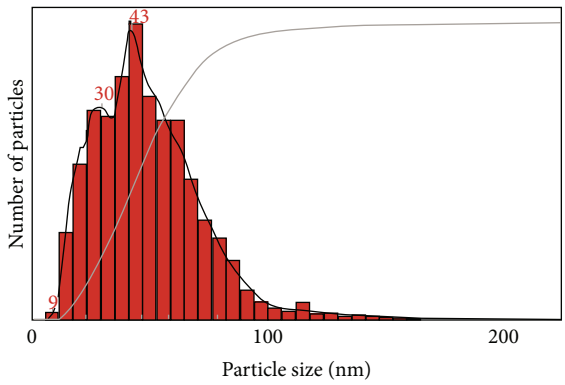

Figure 6: Particle size distribution of C doped ZnO prepared at 300°C.

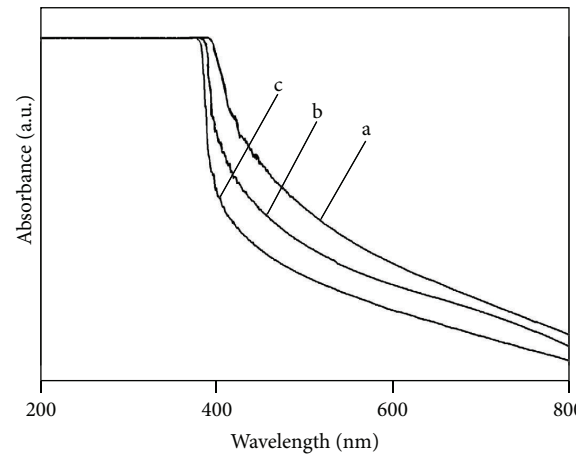

Figure 7: UV-visible absorption spectra of ZnO prepared at (a) 300, (b) 400, and (c) 500°C.

MG. Mechanism of this degradation can be explained as follows:

$$\text{C–ZnO} + h\nu \longrightarrow e^{-}_{CB} + h^{+}_{VB} \quad (2)$$

$$e^{-}_{CB} + h^{+}_{VB} \longrightarrow \text{C–ZnO} + \text{heat} \quad (3)$$

$$e^{-}_{CB} + O_{2(\text{adsorbed})} \longrightarrow O_2^{-\bullet} \quad (4)$$

$$h^{+}_{VB} + H_2O_{(\text{adsorbed})} \longrightarrow H^{+} + HO^{\bullet} \quad (5)$$

$$h^{+}_{VB} + HO^{-}_{(\text{adsorbed})} \longrightarrow HO^{\bullet} \quad (6)$$

$$OH^{\bullet} \text{ or } h^{+}_{VB} + MG \longrightarrow MG^{+\bullet} \longrightarrow \text{Oxidized} \quad (7)$$

Figure 9 shows that in presence of photocatalyst ~98% MG is degraded in 60 min.

Several parameters affect the rate of photocatalytic degradation. To optimize the photocatalysis process it is necessary to study these parameters. Various parameters such as calcination temperature, amount of catalyst, pH, and concentration of MG which affect the rate of photocatalytic degradation were studied and are explained in the following section.

3.9.1. Effect of Calcination Temperature of Catalyst. MG solution was exposed to visible light in presence of pure and C doped ZnO. The UV-visible spectra of the MG

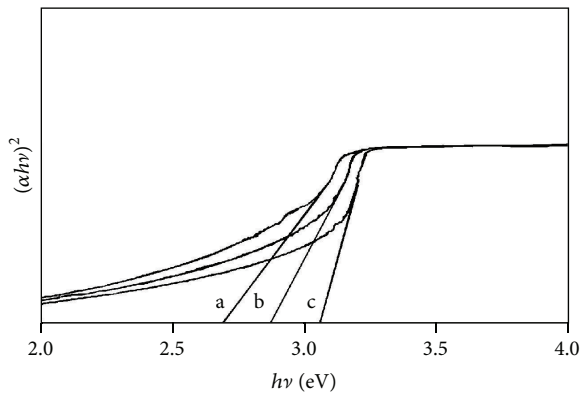

Figure 8: Tauc plots, $(\alpha h\nu)^2$ versus photon energy ($h\nu$) for ZnO prepared at (a) 300, (b) 400, and (c) 500°C.

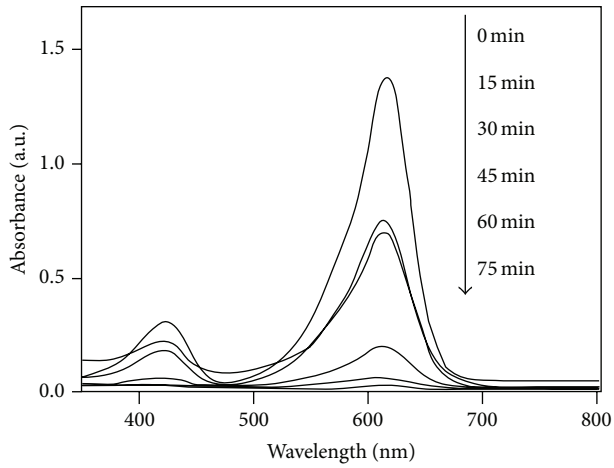

Figure 9: UV-visible spectra of MG solution irradiated with visible light at different time intervals in presence of C doped ZnO photocatalyst prepared at 300°C.

solution exposed for different time intervals were recorded and amount of MG degraded was calculated. The plot of concentration of MG as a function of irradiation time in presence of different catalyst is presented in Figure 10. This figure shows that solution kept in dark for 30 min in presence of catalyst calcined at different temperatures exhibits totally different behavior. Adsorption efficiencies of photocatalyst calcined at 300, 400, and 500°C are 40.8, 23.2, and 8.1%, respectively. It was observed that, as compared to pure ZnO, C doped ZnO showed higher adsorption efficiency for MG dye in dark and this may be due to the enhancement in the adsorption of organic pollutant assisted by doped C. The adsorption of the dye increases with increasing the C content. In absence of catalyst no appreciable degradation of MG was observed even up to 180 min, which means MG is fairly stable to visible light irradiation. Photodegradation efficiency of ZnO decreases with increasing the calcination temperature of catalyst. As the calcination temperature increases C content in ZnO decreases. The catalyst calcined at 300°C gives better photocatalytic activity, reaching ~98% within 60 min. The catalyst calcined at 400 and 500°C degrades ~84 and 67% MG

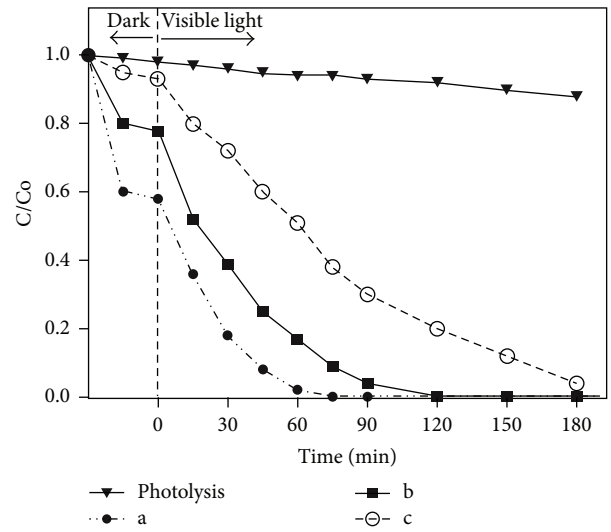

Figure 10: Effect of calcination temperature of catalyst on photodegradation rate of MG catalyst calcined at (a) 300, (b) 400, and (c) 500°C.

within 60 min. This can be due to difference in size and shape as well as C content doped on ZnO at different temperatures. The photodegradation efficiency of MG using photocatalyst calcined at different temperatures is estimated and presented in Table 1.

3.9.2. Effect of Catalyst Loading. Effect of photocatalyst dose on photodegradation of MG dye was investigated using different amount of C doped ZnO photocatalyst obtained at 300°C. For this study the amount of C doped ZnO was varied from 0.1 to 1.0 gL^{-1}. The concentration of MG used to study the dose of catalyst was kept constant at 10 ppm and pH was adjusted to 7. Photocatalytic degradation of MG as a function of irradiation time in presence of varying amount of catalyst was investigated and the data obtained is presented graphically in Figure 11. The graph clearly indicates that as the amount of photocatalyst in the MG solution increases rate of photodegradation increases. At 0.5 gL^{-1} concentration better photocatalytic activity was observed degrading ~98% MG within 60 min. Further increase in the amount of photocatalyst showed decrease in the photodegradation rate. Photodegradation rate depends on presence of surface active sites. If the catalyst loading increased rate of generation of electron/hole pairs and degradation of pollutants increases. However, further increase in the concentration of the catalyst leads to aggregation affecting the number of active sites available for generation of electron/hole pairs. Also, when concentration of catalyst is more photonic flux within irradiated solution decreases which reduces the degradation rate [28].

3.9.3. Effect of pH. Photodegradation process is also strongly affected by pH of the solution. Effect of pH of MG solution on photocatalytic degradation rate was studied and rate constant of photodegradation process as a function of pH of solution

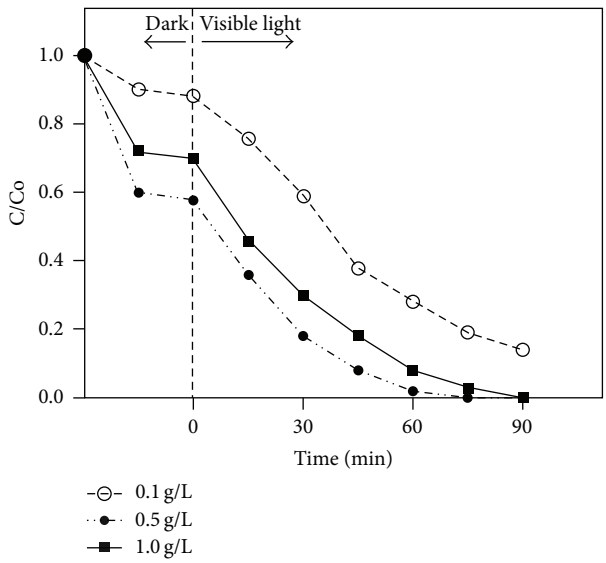

Figure 11: Effect of amount of catalyst on photodegradation rate of MG.

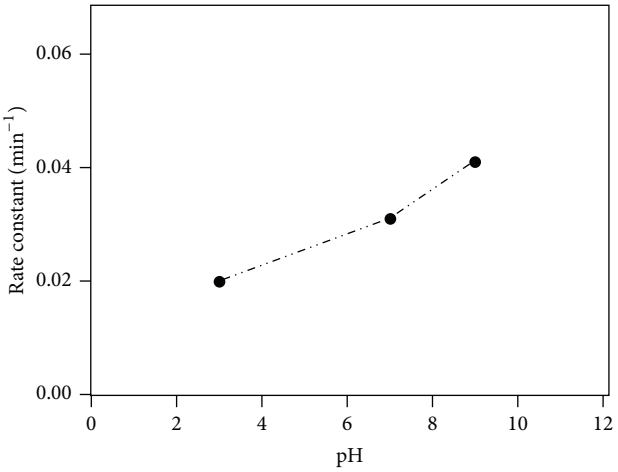

Figure 12: Photodegradation rate of MG as function of pH.

is plotted and presented in Figure 12. The figure indicates that photodegradation efficiency of MG is less at lower pH values and increases with increase in pH. At pH = 9 almost 100% dye degrades within 45 min. In acidic conditions, it is difficult for cationic dye to get adsorbed on catalyst surface. Also at low pH concentration of active $^{\bullet}OH$ radicals is usually low; therefore photodegradation rate of MG remains slow. At high pH formation of active $^{\bullet}OH$ radicals favors due to improved transfer of holes and increases the photodegradation rate.

3.9.4. Effect of Dye Concentration. Effect of dye concentration on MG photodegradation rate was studied by varying the concentrations of MG and keeping the amount of catalyst and pH constant (i.e., 0.5 gL^{-1} and 7, resp.). Photocatalytic data obtained by varying the concentration of MG is presented in Figure 13. As seen in the figure, degradation efficiency is inversely affected by dye concentration. This is because, as the

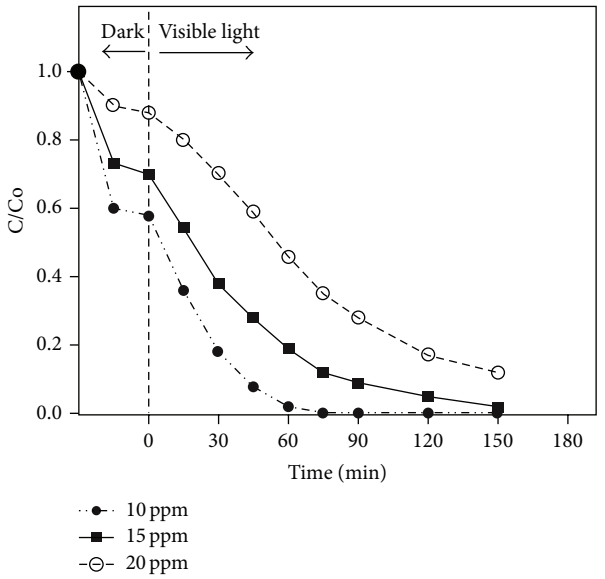

Figure 13: Effect of initial concentration of MG on the photodegradation rate.

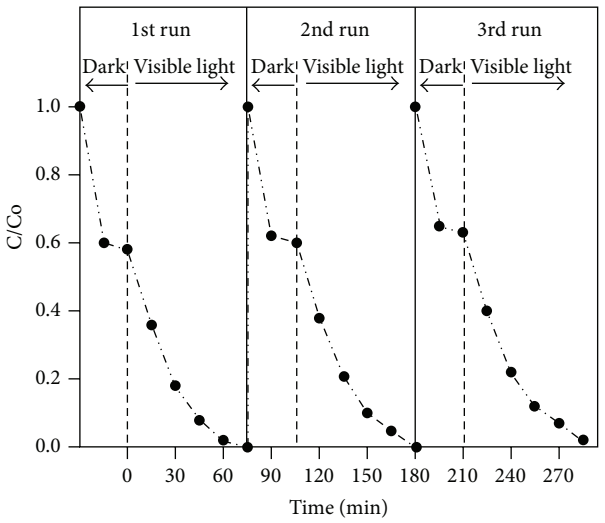

Figure 14: Reuse of photocatalyst up to third cycle.

dye concentration increases, adsorption of dye on the catalyst surface sites increases by decreasing OH^{-} concentration on the same sites. Also according to Beer-Lambert's law, as initial dye concentration increases, the intensity of photons entering the solution decreases which results in lowering the absorption of photons on catalyst surface; hence the rate of photodegradation process decreases.

3.10. Recycling of Photocatalyst. For practical applications stability of photocatalyst during photodegradation is a crucial factor. C doped ZnO prepared at 300°C exhibits better photocatalytic activity; therefore its stability was studied. Stability tests were performed by repeating the reaction three times using recovered photocatalyst. The data obtained is presented in Figure 14. The data reveals that there is no

noticeable decrease in photocatalytic activity up to third cycle, which indicates that C doped ZnO prepared in the present work is highly stable and reusable photocatalyst.

4. Conclusion

C doped ZnO nanorods were synthesized successfully by microemulsion method and have been confirmed to be visible light active and exhibit better photocatalytic activity than pure ZnO due to its decreased band gap (2.69 eV). Photocatalytic activity of ZnO increases with increase in C content. Enhanced photocatalytic activity under visible light irradiation can be attributed to the effect of C doping on ZnO and the major role of C as a channel in reducing the recombination of electron and hole pairs.

Also, it is observed that photocatalytic efficiency does not change up to third cycle and catalyst is quiet stable.

Conflict of Interests

The authors declare that there is no conflict of interests regarding the publication of this paper.

Acknowledgment

The authors are thankful to SAIF, IIT Bombay, for recording SEM and TEM images of sample.

References

[1] G. Liu, H. G. Yang, X. Wang et al., "Enhanced photoactivity of oxygen-deficient anatase TiO_2 sheets with dominant 001 facets," *Journal of Physical Chemistry C*, vol. 113, no. 52, pp. 21784–21788, 2009.

[2] M. Liu, L. Piao, W. Lu et al., "Flower-like TiO_2 nanostructures with exposed 001 facets: facile synthesis and enhanced photocatalysis," *Nanoscale*, vol. 2, no. 7, pp. 1115–1117, 2010.

[3] N. Morales-Flores, U. Pal, and E. S. Mora, "Photocatalytic behavior of ZnO and Pt-incorporated ZnO nanoparticles in phenol degradation," *Applied Catalysis A: General*, vol. 394, no. 1-2, pp. 269–275, 2011.

[4] X. F. Chen, X. C. Wang, and X. Z. Fu, "Hierarchical macro/mesoporous TiO_2/SiO_2 and TiO_2/ZrO_2 nanocomposites for environmental photocatalysis," *Energy and Environmental Science*, vol. 2, no. 8, pp. 872–877, 2009.

[5] A. Akyol, H. C. Yatmaz, and M. Bayramoglu, "Photocatalytic decolorization of Remazol Red RR in aqueous ZnO suspensions," *Applied Catalysis B: Environmental*, vol. 54, no. 1, pp. 19–24, 2004.

[6] C. Lizama, J. Freer, J. Baeza, and H. D. Mansilla, "Optimized photodegradation of reactive blue 19 on TiO_2 and ZnO suspensions," *Catalysis Today*, vol. 76, no. 2–4, pp. 235–246, 2002.

[7] B. Dindar and S. Içli, "Unusual photoreactivity of zinc oxide irradiated by concentrated sunlight," *Journal of Photochemistry and Photobiology A: Chemistry*, vol. 140, no. 3, pp. 263–268, 2001.

[8] Y. Hao, M. Yang, W. Li, X. Qiao, L. Zhang, and S. Cai, "Photoelectrochemical solar cell based on ZnO/dye/polypyrrole film electrode as photoanode," *Solar Energy Materials and Solar Cells*, vol. 60, no. 4, pp. 349–359, 2000.

[9] C. Kormann, D. W. Bahnemann, and M. R. Hoffmann, "Environmental photochemistry: is iron oxide (hematite) an active photocatalyst? A comparative study: α-Fe_2O_3, ZnO, TiO_2," *Journal of Photochemistry and Photobiology A: Chemistry*, vol. 48, no. 1, pp. 161–169, 1989.

[10] J. G. Yu and X. X. Yu, "Hydrothermal synthesis and photocatalytic activity of zinc oxide hollow spheres," *Environmental Science and Technology*, vol. 42, no. 13, pp. 4902–4907, 2008.

[11] Z. Dong, X. Lai, J. E. Halpert et al., "Accurate control of multishelled ZnO hollow microspheres for dye-sensitized solar cells with high efficiency," *Advanced Materials*, vol. 24, no. 8, pp. 1046–1049, 2012.

[12] J. Jiang, X. Zhang, P. Sun, and L. Zhang, "ZnO/BiOI heterostructures: photoinduced charge-transfer property and enhanced visible-light photocatalytic activity," *Journal of Physical Chemistry C*, vol. 115, no. 42, pp. 20555–20564, 2011.

[13] V. Jeena and R. S. Robinson, "Convenient photooxidation of alcohols using dye sensitised zinc oxide in combination with silver nitrate and TEMPO," *Chemical Communications*, vol. 48, no. 2, pp. 299–301, 2012.

[14] H. Ma, J. Han, Y. Fu, Y. Song, C. Yu, and X. Dong, "Synthesis of visible light responsive ZnO-ZnS/C photocatalyst by simple carbothermal reduction," *Applied Catalysis B: Environmental*, vol. 102, no. 3-4, pp. 417–423, 2011.

[15] S. Anandan and M. Miyauchi, "Ce-doped ZnO ($Ce_xZn_{1-x}O$) becomes an efficient visible-light-sensitive photocatalyst by co-catalyst (Cu^{2+}) grafting," *Physical Chemistry Chemical Physics*, vol. 13, no. 33, pp. 14937–14945, 2011.

[16] H. Chen, W. Wen, Q. Wang et al., "Preparation of $(Ga_{1-x}Zn_x)(N_{1-x}O_x)$ photocatalysts from the Reaction of NH_3 with Ga_2O_3/ZnO and $ZnGa_2O_4$: in situ time-resolved XRD and XAFS studies," *Journal of Physical Chemistry C*, vol. 113, no. 9, pp. 3650–3659, 2009.

[17] A. B. Patil, K. R. Patil, and S. K. Pardeshi, "Ecofriendly synthesis and solar photocatalytic activity of S-doped ZnO," *Journal of Hazardous Materials*, vol. 183, no. 1–3, pp. 315–323, 2010.

[18] H. Qin, W. Li, Y. Xia, and T. He, "Photocatalytic activity of heterostructures based on ZnO and N-doped ZnO," *ACS Applied Materials and Interfaces*, vol. 3, no. 8, pp. 3152–3156, 2011.

[19] N. Morales-Flores, U. Pal, and E. S. Mora, "Photocatalytic behavior of ZnO and Pt-incorporated ZnO nanoparticles in phenol degradation," *Applied Catalysis A: General*, vol. 394, no. 1-2, pp. 269–275, 2011.

[20] R. Comparelli, E. Fanizza, M. L. Curri, P. D. Cozzoli, G. Mascolo, and A. Agostiano, "UV-induced photocatalytic degradation of azo dyes by organic-capped ZnO nanocrystals immobilized onto substrates," *Applied Catalysis B: Environmental*, vol. 60, no. 1-2, pp. 1–11, 2005.

[21] L. W. Zhang, H. Y. Cheng, R. L. Zong, and Y. F. Zhu, "Photocorrosion suppression of ZnO nanoparticles via hybridization with graphite-like carbon and enhanced photocatalytic activity," *Journal of Physical Chemistry C*, vol. 113, no. 6, pp. 2368–2374, 2009.

[22] L.-C. Chen, Y.-J. Tu, Y.-S. Wang, R.-S. Kan, and C.-M. Huang, "Characterization and photoreactivity of N-, S-, and C-doped ZnO under UV and visible light illumination," *Journal of Photochemistry and Photobiology A: Chemistry*, vol. 199, no. 2-3, pp. 170–178, 2008.

[23] S. Liu, C. Li, J. Yu, and Q. Xiang, "Improved visible-light photocatalytic activity of porous carbon self-doped ZnO nanosheet-assembled flowers," *CrystEngComm*, vol. 13, no. 7, pp. 2533–2541, 2011.

[24] P. Zhang, C. Shao, Z. Zhang et al., "TiO_2@carbon core/shell nanofibers: controllable preparation and enhanced visible photocatalytic properties," *Nanoscale*, vol. 3, no. 7, pp. 2943–2949, 2011.

[25] P. Zhang, C. Shao, Z. Zhang et al., "Core/shell nanofibers of TiO_2@carbon embedded by Ag nanoparticles with enhanced visible photocatalytic activity," *Journal of Materials Chemistry*, vol. 21, no. 44, pp. 17746–17753, 2011.

[26] N. M. Flores, U. Pal, R. Galeazzi, and A. Sandoval, "Effects of morphology, surface area, and defect content on the photocatalytic dye degradation performance of ZnO nanostructures," *RSC Advances*, vol. 4, no. 77, pp. 41099–41110, 2014.

[27] A. E. Jiménez-González, J. A. S. Urueta, and R. Suárez-Parra, "Optical and electrical characteristics of aluminum-doped ZnO thin films prepared by solgel technique," *Journal of Crystal Growth*, vol. 192, no. 3-4, pp. 430–438, 1998.

[28] M. A. Fox and M. T. Dulay, "Heterogeneous photocatalysis," *Chemical Reviews*, vol. 93, no. 1, pp. 341–357, 1993.